Article

Journal of
Nanoscience and Nanotechnology
Vol. 19, 1480–1484, 2019
www.aspbs.com/jnn

Electron Beam Irradiated Al Doped ZnO Thin Films as Efficient Tunnel Recombination Junction for Hydrogenated Amorphous Silicon/Cu(In,Ga)Se_2 Tandem Solar Cells

Sunhwa Lee[1], Chae-Woong Kim[4], Youn-Jung Lee[1], Jinjoo Park[1], Youngkuk Kim[1], Chaehwan Jeong[3,*], and Junsin Yi[1,2,*]

[1]*School of Information and Communication Engineering, Sungkyunkwan University, Suwon 16419, Korea*
[2]*Department of Energy Science, Sungkyunkwan University, Suwon 16419, Korea*
[3]*Applied Optics and Energy R&BD Group, Korea Institute of Industrial Technology, Gwangju 61012, Korea*
[4]*R&D Center, ISAC Research Inc, Daejeon 34036, Korea*

A tunnel recombination junction (TRJ) layer for hydrogenated amorphous silicon (a-Si:H)/ Cu(In,Ga)Se_2 (CIGS) tandem solar cells is investigated. An Al-doped zinc oxide (AZO) thin film is applied to the TRJ, and the influence of electron beam (e-beam) irradiation on defects along the TRJ is investigated. The AZO thin films are prepared using radio frequency (RF) sputtering and the e-beam is irradiated at 200 W RF power and 2 keV DC power for 5 min. In the e-beam irradiated AZO thin film, the number of oxygen vacancies and Zn interstitials increases, which in turn strengthens the effect of defect-enhanced tunnel recombination.

Keywords: Electron Beam, Tandem Solar Cells, Tunnel Recombination Junction Layer, Al Doped ZnO, Cu(In,Ga)Se_2, Silicon.

1. INTRODUCTION

The growing interest in new types of tandem solar cells such as a-Si:H/Cu(In,Ga)Se_2 (CIGS) tandem solar cells arises from the need for reducing costs associated with high-efficiency multijunction solar cells. a-Si:H/ CIGS tandem solar cells are suitable alternatives for the aforesaid purpose. a-Si:H thin-film solar cells with a thin absorber layer having a high absorption coefficient can be fabricated in a short wavelength region using a low-temperature process and a flexible substrate. The CIGS solar cell holds the current world record for thin-film solar cells with the highest efficiency of 22.6%.[1] The band gap of this material is tunable from 1.02 eV ($CuInSe_2$) to 1.68 eV ($CuGaSe_2$). For tandem cells, the maximum theoretical efficiency is calculated to be 46% with a band gap tunability from 0.94 eV to 1.60 eV. Although chalcopyrite-based top cells for tandem applications have been investigated for more than 30 years, their use has not yet achieved the theoretical potential.[2–4] Other challenges include providing ideal interlayers such as recombination layers or tunnel junctions to assure minimal added series resistance and parasitic optical absorption. For interlayers, materials with a wide band gap, low sub-band-gap optical absorption, appropriate optical refractive index and work function, and high carrier density ($>10^{19}$ cm^{-3}) should be used.

In the present work, we studied tunnel recombination junctions (TRJs) using Al-doped zinc oxide (AZO), known to be in the front transparent electrode of CIGS solar cells, in a-Si:H/CIGS tandem solar cells. This TRJ layer induces effective defect-enhanced tunnel recombination upon electron beam (e-beam) irradiation. e-Beam irradiation increases defect sites in the AZO thin film, decreases cell resistivity, and increases the band gap. Increased defects in the AZO thin film lead to accumulation of charge carriers, thereby forming an electric field at the junction of the bottom cell and top cell, resulting in effective tunneling.

*Authors to whom correspondence should be addressed.

 1533-4880/2019/19/1480/005 doi:10.1166/jnn.2019.16259

2. EXPERIMENTAL DETAILS

AZO thin films were deposited on Corning glass by radio frequency (RF) magnetron sputtering system with a base pressure of 7×10^{-7} Torr at room temperature. The sputtering power and working pressure were optimized at 200 and 1 mTorr, respectively. The as-deposited AZO thin films were irradiated with e-beam at 200 W of RF power and 2 kV of DC power for 5 min.

CIGS bottom cell was grown on Soda-lime glass substrates. These substrates were ultrasonically cleaned with acetone, ethanol and de-ionized water. On etch substrate, a 900-nm-thick bi-layer molybdenum back contact was deposited by DC sputtering system. A CIGS absorber was deposited using three-stage process by co-evaporator. The process temperature was kept at 500 °C. The CIGS absorber was measured by X-ray fluorescence (XRF), showing a compositional ratio of $Cu/(In + Ga) = 1.1$ and $Ga/(In + Ga) = 0.25$. CdS was deposited via chemical bath deposition at 60 °C. An intrinsic zinc oxide with a thickness of 50 nm was deposited using the RF sputtering system. An AZO TRJ of 50 nm was deposited by the RF magnetron sputtering system.

An a-Si:H top cell was deposited using an RF plasma enhanced chemical vapor deposition (RF PECVD, 13.56 MHz) technique. The top cell was deposited with an absorber layer of a thickness of 350 nm. Front transparent conductive oxide (TCO) was deposited using the RF sputtering system, and the top Al grid electrode was deposited by thermal evaporation system. The structural properties of the AZO thin films were investigated by X-ray diffraction (XRD, X'pert-Pro, Panalytical), scanning electron microscopy (SEM, SNE4500N, SEC). The optical and electrical properties of the AZO thin films were investigated using a UV-Visible spectrometer (Carry 500, Varian Inc.) and Hall effect measurement system (7700A, Lakeshore). The solar cell characteristics were measured with a solar simulator (Wacom, WXS-105H) calibrated to 1 sun and 100 mW/cm^2. The external quantum efficiency (EQE) of the solar cell was measured by a QEX7 system (PV Measurements Inc.).

3. RESULTS AND DISCUSSION

3.1. Properties of Electron Beam

Figure 1(a) shows the electron dose values for different DC and RF powers of the e-beam. RF power generates the plasma, and DC power accelerates the electrons. The electron dose was investigated using an energy analyzer. Figure 1(b) shows a schematic of the energy analyzer. The electron dose was increased from 3.5×10^{16} to 1.5×10^{17} electron/cm^2 by increasing the DC power of the e-beam. For RF power, the electron dose was saturated to 8.97×10^{16} electron/cm^2 at 200 W. When electrons were generated above a certain level by the RF power, they were affected by the DC power accelerating the electrons rather than the actual number of generated electrons.

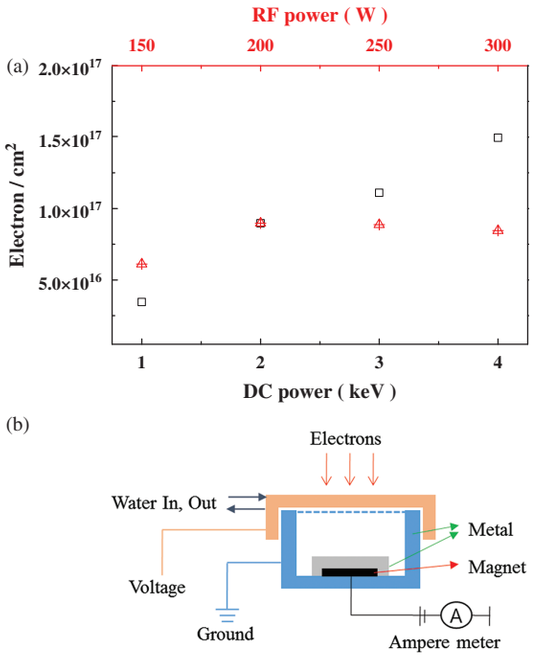

Figure 1. Change in electron concentration when RF and DC power of electron beam are varied (a) and the schematic diagram of energy analyzer (b).

3.2. Properties of AZO Thin Films

Figure 2 shows SEM images of the surface grain structure of the as-deposited and e-beam irradiated AZO thin films. The film grew with a columnar structure, consistent with the XRD results shown in Figure 2(e) (*c*-axis orientation). After e-beam irradiation, the AZO thin film showed strong peaks corresponding to the preferred (002) orientation.[5] The full-width at half-maximum of the XRD (002) peaks decreased from 0.4° to 0.2° upon e-beam irradiation with 2 keV DC power and 200 W RF power. The crystallinity and grain size increased with e-beam irradiation. From the above results, we found that the preferred (002) orientation of the AZO thin films increased with e-beam irradiation. It is known that e-beam irradiation of the solids and thin films can activate and control adsorption–desorption processes by modification of their surface chemistry. e-Beam irradiation onto solids may affect elementary reactions of excitation, ionization, and dissociation. e-Beam irradiation involves three stages. First, the physical stage during 10^{-10} s leads to excitation of the molecules on interaction with a "hot" particle and dissociation of the irradiated molecules into ion radicals or ions and electrons within the time about the period of intra-molecular vibrations. Second, the physicochemical stage during 10^{-13} to 10^{-10} s involves the reaction between charged and excited particles as well as energy transfer processes. Finally, the chemical stage during the period depends on gas phase composition and thermodynamic parameters.[6]

Table I shows the optical and electrical parameters of the as-deposited and e-beam irradiated AZO thin films.

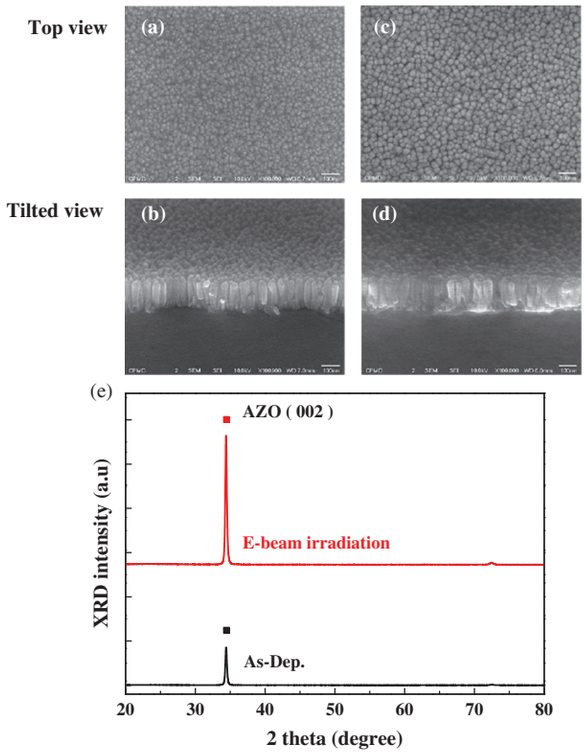

Figure 2. Top views and tilted views of AZO thin films: as-deposited (a, b) after e-beam irradiation (c, d) and XRD patterns of AZO thin films of as-deposited and after e-beam irradiation (e).

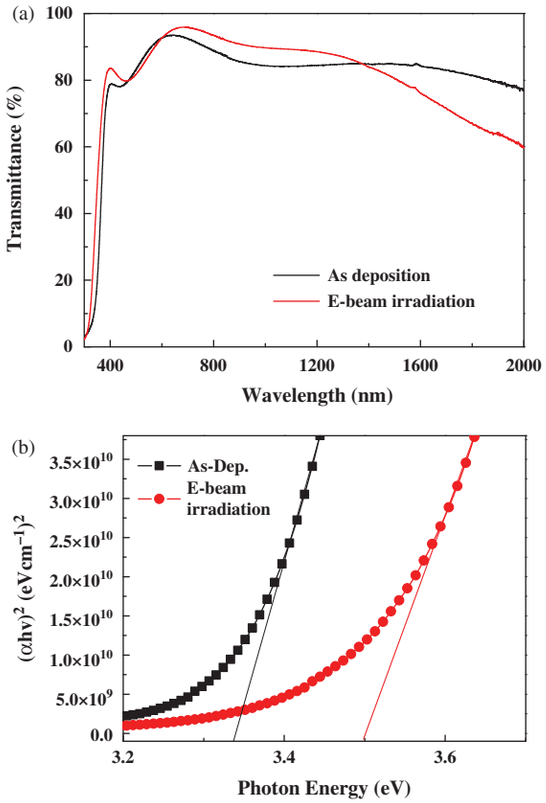

Figure 3. Transmittance spectra (a) and Tauc plots (b) of as-deposited and E-beam irradiated AZO thin films.

The resistivity decreased from 8.84×10^{-4} to 4.73×10^{-4} Ωcm during e-beam irradiation. The decrease in resistivity resulted from the increased carrier concentration and improved hole mobility. The hole mobility increased from 15.3 to 25.4 cm/V·s and was mainly limited by grain boundary scattering.[7, 8] The decreased grain boundary scattering was due to the increased grain size, as demonstrated by the XRD and SEM results. After e-beam irradiation, the optical band gap shifted to a higher energy level (blue shift), from 3.34 to 3.5 eV, which could be attributed to the Moss-Burstein (MB) effect.[9, 10] The Fermi level moved into the conduction band of the degenerate semiconductor because of the increase in electron concentration caused by Al dopants, resulting in widening of the optical band gap. As shown in Figure 3(a), because of e-beam irradiation, the transmittance of the AZO thin films shifted to a lower wavelength and that of the NIR region decreased on account of free electron absorption. The optical and electrical properties of the AZO thin films, as listed in Table I

Table I. The electrical and optical properties of AZO thin films.

	Resistivity (ohm·cm)	Mobility (cm/V·s)	Concentration (#/cm^3)	Transmittance (%)	Band gap (eV)
As-Dep.	8.84×10^{-04}	15.3	3.26×10^{20}	87.49	3.34
E-beam irradiation	4.73×10^{-04}	25.4	5.2×10^{20}	89.52	3.50

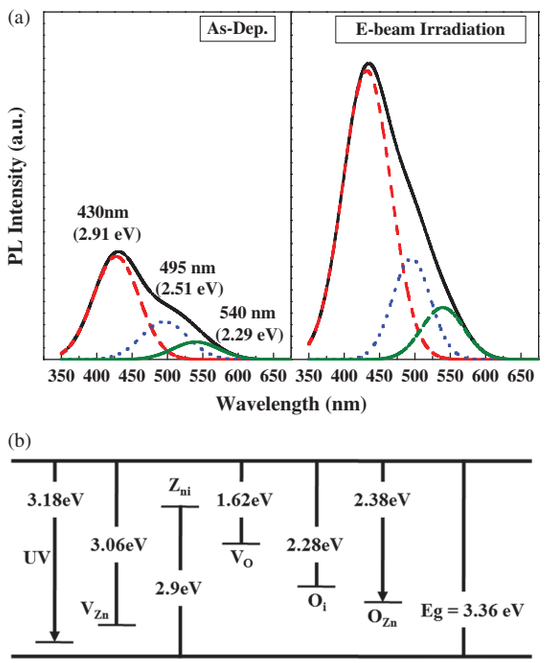

Figure 4. Deconvoluted PL spectra of AZO thin films of as-deposited and with e-beam irradiation (a) and defect levels in ZnO film (b).

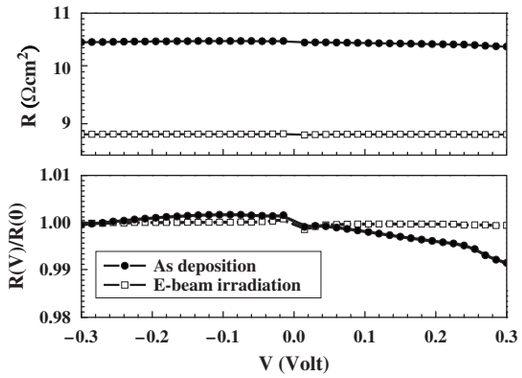

Figure 5. Voltage dependence of resistance (top), Resistance normalized by the resistance value at 0 volts (bottom). The measurements were carriered out at RT.

and Figure 3, indicate an increase in carrier concentration upon e-beam irradiation, leading to optical band gap widening due to the MB effect.[11, 12]

Figure 4(a) shows the deconvoluted PL spectra of the AZO thin films with Gaussian function. Three deep-level emission bands, with one sharp peak at approximately 430 nm (2.91 eV; blue emission) and two broad peaks located at approximately 495 nm (2.51 eV) and 540 nm (2.29 eV; green emission), were observed in the case of the as-deposited and e-beam irradiated AZO thin films. The deep-level emissions were probably related to variations in the defects. The calculation results are shown in Figure 4(b). The energy interval from the Zn interstitial levels to the top of the valence band was approximately 2.9 eV and that to the Zn vacancy levels was approximately 2.6 eV. The blue emission was assigned to the electron transition from the Zn interstitial levels to the top of the valence band and to the Zn vacancy levels. After e-beam irradiation, the PL spectrum intensity, 430 nm (2.91 eV), was increased by Al^{3+} substitution. The increase in Al^{3+} content led to increasing Zn interstitial levels because ZnO is a self-assembled oxide compound. Al^{3+} might act as an acceptor in the AZO thin films.[13] According to Figure 4(b), the interstitial oxygen Oi level (2.28 eV) could be attributed to electron transition from the bottom of the conduction band. The interstitial oxygen Oi played the role of an acceptor in the AZO thin

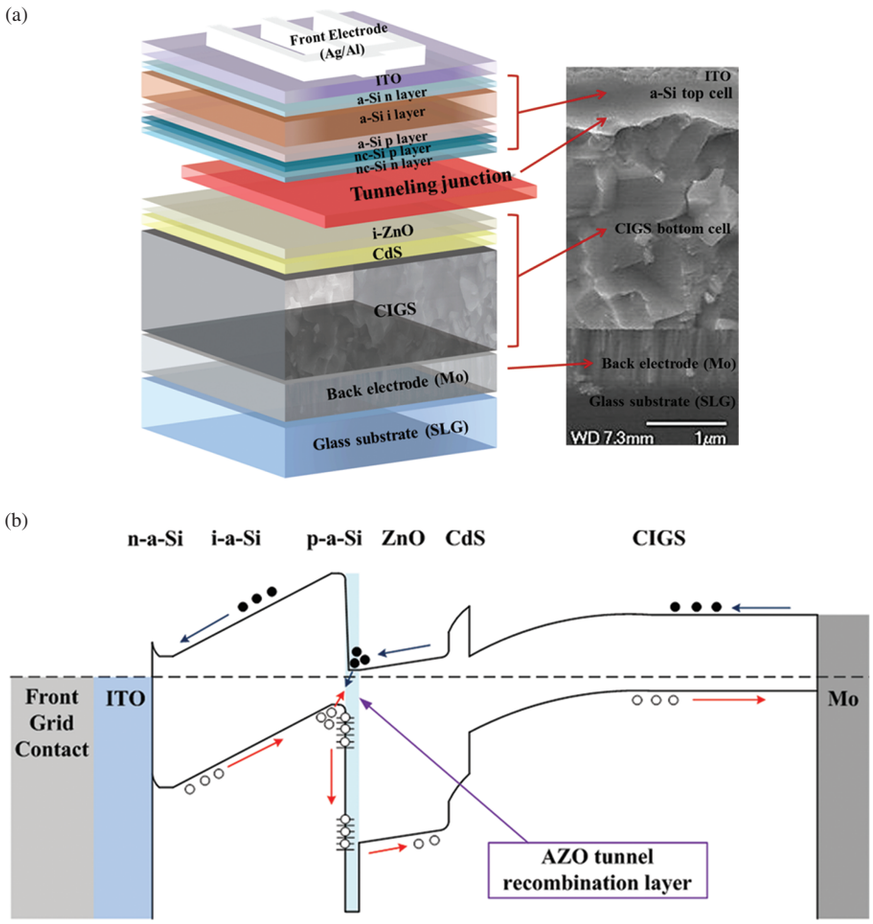

Figure 6. (a) Schematic diagram of a-Si:H/CIGS tandem solar cell (left) and cross-sectional SEM image (right). (b) Band diagram of a-Si:H/CIGS tandem solar cell with e-beam irradiated AZO showing the defect-enhanced tunnel recombination.

Table II. The device parameters of a-Si:H/CIGS tandem solar cells.

	Device	J_{sc} (mA/cm^2)	V_{oc} (V)	FF (%)	Eff (%)
Tandem cell	AZO TJ				
	As-dep.	7.9	0.61	26.7	1.29
	E beam irradiation	8.35	1.01	37.8	3.14

films. The deep-level emission of the AZO thin films was related to electron transition from the bottom of the conduction band to the interstitial oxygen Oi level. The green emission at 495 nm (2.51 eV) and 540 nm (2.29 eV) originated from electron transition from the oxygen vacancy level to the valence band. After e-beam irradiation, blue emission and green emission peaks increased. Because of these defects, the AZO thin film can be used as an effective defect-enhanced TRJ.

3.3. Tunnel Recombination Properties and Solar Cell Characterization

Figure 5 shows the voltage dependence of the resistance (R) for the TRJ. The as-deposited TRJ shows non-ohmic behavior, and e-beam irradiated TRJ shows an ohmic behavior. As described in Figure 4, defects of the AZO thin film are increased by e-beam irradiation. Due to the increased defects, defect-enhanced tunneling occurs and the ohmic behavior to TRJ can be obtained. In the as-deposited AZO thin film, the ohmic behavior is difficult to obtain because the defects are not sufficient to cause the tunneling current. The structure and cross-sectional SEM images of a-Si:H/CIGS tandem solar cells are shown in Figure 6(a). The cells were all processed under the same conditions, with the only variation being the use of e-beam irradiation in the AZO TRJ. As shown in Table II, the fill factor was higher upon e-beam irradiation, and Jsc and Voc increased. The a-Si:H/CIGS tandem cell required optimization of the front transparent electrode and absorber layer thickness of the top and bottom cells, stability, and transparency. Figure 6(b) shows the band diagram of an a-Si:H/CIGS tandem solar cell with the e-beam-irradiated AZO TRJ. Increased defects in the AZO thin films led to the accumulation of charge carriers to form an electric field, thereby causing electron transfer from the bottom cell to the top cell and hole transfer from the top cell to the bottom cell. The EQE spectra of the a-Si:H/CIGS tandem solar cell with the AZO TRJ is shown in Figure 7. With the as-deposited AZO thin films, EQE spectra were not clearly distinguishable because the TRJ was not appropriately formed in the tandem solar cell. However, after e-beam irradiation, the EQE spectra increased and subcells were clearly distinguishable.

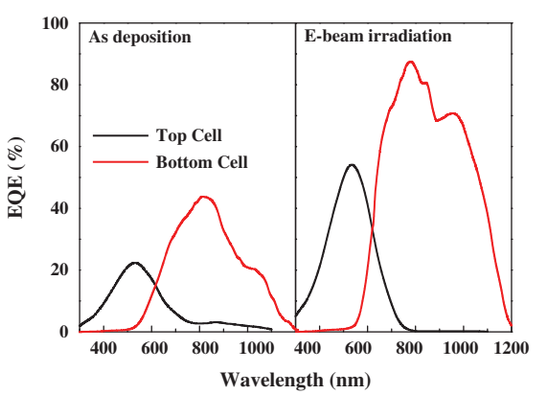

Figure 7. EQE spectra of a-Si:H/CIGS tandem solar cell.

4. CONCLUSION

In summary, AZO thin films have been grown by RF magnetron sputtering and the effects of e-beam irradiation were studied. It was found that the interstitial oxygen and interstitial zinc were increased with the e-beam irradiation. These oxygen and zinc act as trap states of charged carrier, defect-enhanced tunneling occurs and the ohmic behavior to TRJ can be obtained. We fabricated a-Si:H/CIGS tandem solar cell with e-beam irradiated AZO tunneling recombination layer. The cell showed V_{oc} of 1.01 V and J_{sc} of 8.35 mA/cm^2.

Acknowledgments: This work was supported by the Korea Institute of Energy Technology Evaluation and Planning (KETEP) and the Ministry of Trade, Industry and Energy (MOTIE) of the Republic of Korea (No. 20163030013760) (No. 20173010012940).

References and Notes

1. M. A. Green, K. Emery, Y. Hishikawa, W. Warta, and E. D. Dunlop, *Prog. Photovolt. Res. Appl.* 24, 3 (**2016**).
2. Z. Jason, Yu, M. Leilaeioun, and Z. Holman, *Nat. Energy* 1, 1 (**2016**).
3. S. P. Bremner, M. Y. Levy, and C. B. Honsberg, *Prog. Photovolt. Res. Appl.* 16, 225 (**2008**).
4. S. P. Bremner, C. Yi, I. Almansouri, A. Ho-Baillie, and M. A. Green, *Sol. Energy* 135, 750 (**2016**).
5. H. X. Chen, J. J. Ding, X. G. Zhao, and S. Y. Ma, *Physica B* 405, 1339 (**2010**).
6. V. S. Vavilov, Effect of Irradiation on Semiconductor, Springer, Boston (**1965**).
7. M. Wang, J. Wang, W. Chen, Y. Cui, and L. Wang, *Mater. Chem. Phys.* 97, 219 (**2006**).
8. Y. C. Liu, S. K. Tung, and J. H. Hsieh, *J. Cryst. Growth* 287, 105 (**2006**).
9. J. P. Lin and J. M. Wu, *Appl. Phys. Lett.* 92, 134103 (**2008**).
10. J. Mass, P. Bhattacharya, and R. S. Katiyar, *Mater. Sci. Eng. B* 103, 9 (**2003**).
11. S. S. Lin, J. L. Huang, and P. Šajglik, *Surf. Coat. Technol.* 185, 254 (**2004**).
12. E. Burstein, *Phys. Rev.* 93, 632 (**1954**).
13. A. F. Kohan, G. Ceder, and D. Morgan, *Phys. Rev. B* 61, 15019 (**2000**).

Received: 17 January 2018. Accepted: 19 March 2018.